ACS Biomaterials SCIENCE & ENGINEERING

pubs.acs.org/journal/abseba

Article

Hydrogel-Supported, Engineered Model of Vocal Fold Epithelium

Anitha Ravikrishnan,[†] Eric W. Fowler,[†] Alexander J. Stuffer, and Xinqiao Jia*

Cite This: https://dx.doi.org/10.1021/acsbiomaterials.0c01741

Read Online

ACCESS | Metrics & More | Article Recommendations | Supporting Information

ABSTRACT: There is a critical need for the establishment of an engineered model of the vocal fold epithelium that can be used to gain understanding of its role in vocal fold health, disease, and facilitate the development of new treatment options. Toward this goal, we isolated primary vocal fold epithelial cells (VFECs) from healthy porcine larynxes and used them within passage 3. Culture-expanded VFECs expressed the suprabasal epithelial marker cytokeratin 13 and intercellular junctional proteins occludin, E-cadherin, and zonula occludens-1. To establish the engineered model, we cultured VFECs on a hyaluronic acid-derived synthetic basement membrane displaying fibronectin-derived integrin-binding peptide (RGDSP) and/or laminin 111-derived syndecan-binding peptide AG73 (RKRLQVQLSIRT). Our results show that matrix stiffness and composition cooperatively regulate the adhesion, proliferation, and stratification of VFECs. Cells cultured on hydrogels with physiological stiffness (elastic shear modulus, G' = 1828 Pa) adopted a cobblestone morphology with close cell−cell contacts, whereas those on softer matrices (G' = 41 Pa) were spindle shaped with extensive intracellular stress fibers. The development of stratified epithelium with proliferating basal cells and additional (1−2) suprabasal layers requires the presence of both RGDSP and AG73 peptide signals. Supplementation of cytokines produced by vimentin positive primary porcine vocal fold fibroblasts in the VFEC culture led to the establishment of 4−5 distinct cell layers. The engineered vocal fold epithelium resembled native tissue morphologically; expressed cytokeratin 13, mucin 1, and tight/adherens junction markers; and secreted basement membrane proteins collagen IV and laminin 5. Collectively, our results demonstrate that stiffness matching, cell−matrix engagement, and paracrine signaling cooperatively contribute to the stratification of VFECs. The engineered epithelium can be used as a versatile tool for investigations of genetic and molecular mechanisms in vocal fold health and disease.

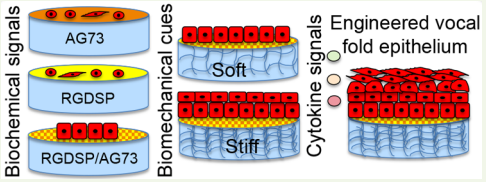

KEYWORDS: *vocal fold epithelial cells, stratification, hydrogel, hyaluronic acid, peptide*

1. INTRODUCTION

When driven into a wavelike motion by the air from the lung, vocal folds produce a variety of sound that is essential to communication. The human vocal fold is composed of a lamina propria sandwiched between a stratified squamous epithelium and the vocalis muscle.[1] The lamina propria is a loose connective tissue sparsely populated by fibroblasts (VFFs).[2,3] Anchored on a basement membrane, the epithelium consists of stacked epithelial cells (VFECs) held together by adherens junctions, desmosomes, and tight junctions, with a cytokeratin 14 (KRT14) positive basal layer and up to six cytokeratin 13 (KRT13) positive suprabasal layers. During tissue turnover, VFECs divide in the basal layer and move superiorly and medially into the suprabasal layers. The outermost luminal cells are eventually replaced with new cells while old cells are sloughed off into the laryngeal lumen. The epithelium maintains tissue hydration, interfaces with the external environment, provides structural stability to the vocal fold, and protects the underlying lamina propria from chemical/immunological irritation and biomechanical trauma. The epithelium, together with the superficial lamina propria, contributes to the propagation of the mucosa wave over the vocal fold during phonation.[4−7]

Vocal folds can be damaged by exposure to chemicals, such as pollutant particles and refluxed stomach acids. Mechanical factors, such as trauma introduced during intubation or stress induced in voice abuse and overuse, can also result in vocal fold scarring.[8] Accumulating knowledge suggests that VFECs play important roles in triggering and sustaining tissue fibrosis.[9,10] Animal studies have shown that, following surgical striping of the epithelium, rapid re-epithelialization is achieved in 3−5 days, yet the epithelial barrier function is not fully recovered.[11] Excessive phonation can lead to destruction of tight/adherens junctions, shedding of surface VFECs, dilation of paracellular spaces, and denudement of the basement membrane. The surviving or newly grown epithelial cells express different cytokeratins, are predisposed to further injury, secrete profibrotic mediators, and promote abnormal repair.[12]

Despite the importance of VFECs in vocal fold homeostasis and diseases, few studies investigate the development of an artificial epithelium that resembles the structure and function of the native tissue. Mizuta et al. cultured rabbit VFECs on collagen IV coated tissue culture plates as a monolayer. To

Special Issue: Advanced Biomedical Hydrogels

Received: December 15, 2020
Accepted: February 19, 2021

establish an epithelial multilayer expressing the epithelial cell markers KRT13, KRT14 and the tight junction proteins occludin, zonula occludens-1 (ZO-1), mouse 3T3 feeder cells were required.[13] Separately, Erickson-DiRenzo et al. cultured porcine VFECs on tissue culture plates as a monolayer. Cells exhibited a cobblestone appearance and were stained positive for pan-cytokeratin and expressed mucins (MUC) 1 and 4 at the transcript level.[14] Although these studies laid the foundation for the development of physiologically relevant vocal fold tissue model, culturing VFECs on rigid tissue culture plates may inadvertently alter cell phenotype. Finally, Ling et al. cultured human VFECs on VFF-populated collagen gels under organotypic conditions.[15] The bioengineered mucosae showed morphologic features of native tissue, proteome-level evidence of mucosal morphogenesis, and emerging extracellular matrix complexity, but did not exhibit mature barrier function.

The goal of this work is to gain a fundamental understanding on how different biochemical and biomechanical signals regulate the attachment, proliferation, and stratification of VFECs. Herein, primary VFECs were isolated from porcine larynxes and the contaminating VFFs were depleted by selective attachment. The epithelial cultures were expanded and characterized by immunostaining for stratified epithelial cell markers and tight/anchoring junction markers, and compared to the native porcine vocal fold tissue. Hyaluronic acid (HA)-based hydrogels of varying HA concentration and presenting fibronectin-derived cell adhesive motif (RGDSP) and laminin 111-derived syndecan binding peptide (AG73)[16] were evaluated for initial cell attachment and proliferation. HA is naturally abundant in the lamina propria, contributing to the maintenance of optimal tissue mechanics.[17−19] In addition, HA binds specific cell surface receptors and directs cell adhesion, wound healing, and tissue morphogenesis.[20,21] Thus, HA-based hydrogels presenting basement membrane protein signals recapitulate the epithelium-mesenchyme tissue boundary, allowing mechanistic interrogation of cell−matrix interactions necessary for VFEC stratification. Further enhancement in stratification was achieved by supplementing the epithelial culture with VFF-conditioned media. The engineered model can be used to investigate cellular events and molecular mechanisms contributing to the development of a disease phenotype.

2. MATERIALS AND METHODS

2.1. Hydrogel Synthesis and Characterization. *2.1.1. Synthesis of Hydrogel Building Blocks.* Acrylate-functionalized HA (HA-AES) was synthesized as previously reported.[22] Briefly, sodium hyaluronate (5 kDa, Lifecore Biomedical, Chaska, MN) was converted to tetrabutylammonium salt and reacted with mono-2-(acryloyloxy)ethyl succinate (AES) in DMSO. Purified product was collected after precipitation, ion-exchange, and dialysis. An acrylate degree of modification of 50% was determined using ^{1}H NMR.[22] Separately, sodium hyaluronate (430 kDa, Sanofi Genzyme Corporation, Cambridge, MA) was reacted with 3,3′dithiobispropanoic dihydrazide in deionized water in the presence of N-(3-(dimethylamino)propyl)-N′-ethylcarbodiimide hydrochloride at pH 4.75 under rigorous mechanical stirring for 1 h. After treatment with 1,4-dithiothreitol, the product was purified by dialysis and lyophilized to produce HA-SH. Characterization by ^{1}H NMR indicated 60% thiol modification.[23]

Maleimide-functionalized peptides MI-GGGRGDSPG[23] and MI-GGGRKRLQVQLSIRT were synthesized on a PS-3 peptide synthesizer (Protein Technologies, Tucson, AZ). Fmoc solid phase synthesis was conducted at 0.25 mmol scale using Rink-Amide MBHA resin (EMD Millipore, Burlington, MA). Maleimide functionality was incorporated by reacting 4-maleimidobutyric acid (1.0 mmol) with the N-terminal glycines using N,N,N′,N′-tetramethyl-O-(1H-benzotriazol-1-yl)uronium hexafluorophosphate (HBTU, 1.0 mmol)/N, N-diisopropylethylamine (DIPEA, 2.0 mmol) in DMF for 1 h to produce RGDSP-MI and AG73-MI. Peptides were cleaved with TFA/TIPS/H_2O (95:2.5:2.5, v/v) and precipitated into diethyl ether. Peptides were purified with reverse phase high-performance liquid chromatography (RP-HPLC). Peptide purity was analyzed at 220/280 nm (Figure S1) using a Shimadzu Prominence Series HPLC (Kyoto, Japan). A Waters UPLC LC-MS/MS system with an ESI source (Xevo G2-S QTof, Milford, MA) was used to confirm peptide mass (Figure S2).

2.1.2. Oscillatory Rheology. HA-SH and HA-AES were separately dissolved in PBS at pH 7.4 and mixed at 20/1 (v/v). Hydrogels prepared using 10 mg/mL HA-SH and 10 mg/mL HA-AES had a final HA concentration of 10 mg/mL (HA10) and those prepared using 20 mg/mL HA-SH and 100 mg/mL HA-AES had a final HA concentration of ∼24 mg/mL (HA24). The viscoelastic properties of HA gels were analyzed using a TA Instruments DHR-3 rheometer (New Castle, DE) with a 12 mm stainless steel geometry and 500 μm gap size at 37 °C. Promptly after mixing, the liquid was loaded on a plate/plate geometry, and mineral oil was applied around the geometry. Time sweep was performed with 1.0% strain at 1 Hz. After 2 h, a frequency sweep from 0.1 to 10 Hz was performed at 1.0% strain. Measurements were conducted in triplicate, and the average storage (G') and loss (G'') moduli are reported.

2.1.3. Characterization of Peptide Conjugation. HA-SH and HA-AES solutions were mixed and aliquoted into 12 mm cell culture inserts. Five minutes later, RGDSP-MI and AG73-MI (100 μL, 0.5 mM each) were added on top of the gel mixture and incubated for 30 min. The supernatant was aspirated and the hydrogel was washed with PBS (100 μL) three times. The supernatant and the wash solutions were pooled and lyophilized for the respective hydrogel. The dry product was dissolved in 100 μL of deionized water and ran on the Shimadzu analytical HPLC by monitoring peptide elution at 220 nm. Pure peptides of known concentrations were analyzed similarly, and standard curves were constructed based on peak integration at each concentration. Peptide concentration in the combined wash solutions was determined using the standard curve.

2.2. Isolation and Characterization of VFECs. *2.2.1. Cell Isolation and Expansion.* Porcine larynxes were collected from healthy Yucatan mini-pigs, (male and female, 4−6 months old). All animal procedures were performed at the Philadelphia VA Medical Center with approval from the Institutional Animal Care and Use Committee and in accordance with policies set forth by the National Institutes of Health. The larynxes were transported in ice cold sterile Hank's balanced salt solution (HBSS, with calcium and magnesium) supplemented with 100 IU/mL penicillin-streptomycin. The larynxes were then dissected along the midsagittal plane, and the true vocal folds were microdissected from its underlying thyroarytenoid muscle. The resected vocal folds were washed with calcium- and magnesium-free HBSS containing 100 IU/mL penicillin-streptomycin (HBSS+) and enzyme digested with 1 U/mL Dispase II (Sigma-Aldrich, St. Louis, MO) in HBSS+ overnight at 4 °C.

After digestion, the epithelium was carefully peeled off the underlying lamina propria and placed in a tube containing HBSS+. The cells were then isolated from the epithelium by incubating with 0.05% (wt/vol) trypsin-EDTA solution for 5 min and neutralized using a trypsin soybean inhibitor (Sigma-Aldrich). The cell suspension was further neutralized and washed with flavonoid adenine dinucleotide (FAD) media containing Ham's F-12/DMEM (3:1 ratio), 100 IU/mL penicillin−streptomycin, fetal bovine serum (2.5%), epidermal growth factor (10 ng/mL), insulin (5 μg/mL), hydrocortisone (0.4 μg/mL), cholera toxin (8.4 ng/mL), and adenine (24 μg/mL).[14]

To prepare flasks for subculture, collagen IV stock solution (Sigma-Aldrich) was diluted in sterile HBSS to a concentration of 50 μg/mL. Two milliliters of the solution was added to a T25 flask, and the flask was incubated at room temperature for 1 h. The flask was washed

https://dx.doi.org/10.1021/acsbiomaterials.0c01741
ACS Biomater. Sci. Eng. XXXX, XXX, XXX−XXX

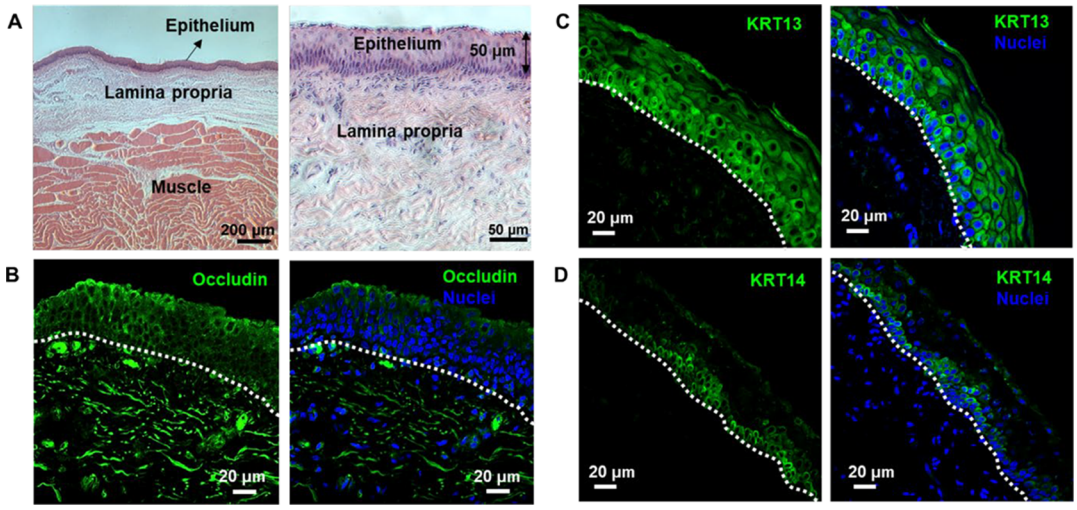

Figure 1. Characterization of porcine vocal folds by (A) H&E and (B–D) immunohistochemistry. Tissues were collected from a 4-month old male pig. (A) The stratified squamous epithelium contained five distinct cell layers with an estimated thickness of 50 μm. (B) Tissues were stained positive for occludin, a tight junction marker. (C) KRT13 expression extended throughout the entire stratified epithelium, sparing some basal cells that were directly attached to the basement membrane. (D) KRT14 labeled the bottom three to four layers of epithelial cells. The right panels in B–D show markers overlaid with nuclei stained by DAPI. White dotted line indicates the basement membrane.

with sterile HBSS prior to cell seeding. The cell suspension was filtered through a 40 μm cell strainer and centrifuged. The supernatant was carefully removed, and the cell pellet was resuspended in FAD media and seeded on collagen IV-coated cell culture flask. Isolated VFECs were cultured in a humidified incubator at 37 °C with 5% CO_2 and 95% air. The growth and morphology of the VFECs were monitored daily and media was replaced every 4 days until they reach 50% confluency and from then every 2 days until they reach full confluency. Before passage, VFECs were plated on uncoated cell culture flask to allow VFFs to attach. After 2 h of incubation, the floating cell population was collected and replated on a collagen IV-coated flask to obtain pure population of VFECs. The attached VFFs were cultured in DMEM supplemented with 10% fetal bovine serum (FBS) and 100 IU/mL penicillin–streptomycin. Experiments in this work were conducted from VFECs within passages 1–3 from at least three different animals.

2.2.2. Growth Kinetics. VFECs were plated on collagen IV-coated tissue culture plates at 4×10^4 cells/cm^2 and VFFs were seeded and maintained on uncoated plates at 5×10^3 cells/cm^2. After 7 days of culture, cells were trypsinized, stained with trypan blue and counted using a hemocytometer. The doubling time was calculated as $2^N = C_f/C_i$, where N is the doubling time, C_i refers to the initial cell count at the time of seeding, and C_f is the final cell count on day 7.

2.2.3. Flow Cytometry. Cells were washed with PBS and stained with FITC-labeled anti-CD90 antibody (BD Biosciences, San Jose, CA) for 15 min at room temperature for cell surface staining. Next, cells were washed with cold PBS and fixed using 0.5% paraformaldehyde (PFA)/0.1% Triton solution at a concentration of 2×10^6 cells/mL. Subsequently, cells were incubated for 10 min and washed with Perm/Wash buffer (BD Biosciences) consisting of 3% bovine serum albumin (BSA) and 0.1% Triton in PBS. Finally, cells were treated with Alexa Fluor 647 monoclonal antibody that recognizes intracellular keratins 14, 15, 16, and 19 (KRT, BD Biosciences) for 30 min and washed using Perm/Wash buffer. Samples were ran using BD FACSAria II instrument (BD Biosciences) and analyzed using *FlowJo* software. Results were compared to their respective IgG controls. Antibody information can be found in Table S1.

2.3. Development of Hydrogel-Supported Epithelium. *2.3.1. Culture of VFECs on HA Gels.* HA hydrogels were prepared as described above in **2.1.3.** using sterile-filtered HA-SH, HA-AES, RGDSP-MI and AG73-MI. VFECs were seeded on the hydrogels at a concentration of 1×10^3 cells/μL. Cultures were submerged in FAD media until a cell monolayer was developed. Thereafter, cultures were maintained at the air–liquid interface, with media present only in the well surrounding the inset, until day 42. Alternatively, the FAD media was replaced with fibroblast-conditioned media produced by culturing VFFs isolated from the same animal in DMEM media at passage 3 until 80% confluency. Media was changed every other day.

2.3.2. Viability Assay. For LIVE/DEAD cell staining, calcein AM (Life Technologies, Carlsbad, CA) and ethidium homodimer-1 (EthD-1, Life Technologies) were diluted at 1:1000 (v/v) and 1:2000 (v/v), respectively, with sterile PBS. After aspirating media and washing with 300 μL of warm PBS, samples were incubated with 300 μL of the dye solution at 37 °C for 20 min. The constructs were assayed after 7, 14, 21, and 42 days of culture using a Zeiss LSM 880 confocal microscope (Oberkochen, Germany). Viability was quantified based on the percentage of calcein positive area using *ImageJ* software.

2.3.3. Immunofluorescence. Cells were fixed with 4% (v/v) PFA in PBS for 20 min. Following a 20 min permeabilization using 0.1% Triton X-100 in a 3% BSA/PBS solution. The Triton solution was rinsed, and nonspecific binding was blocked with 3% BSA for 1 h at room temperature. Samples were incubated with primary antibodies (Table S1) diluted in 3% BSA (1:100) at room temperature for 2 h. After rinsing, samples were incubated with secondary antibodies, Alexa Fluor 488 goat antimouse (Thermo Fisher Scientific, Waltham, MA), and Alexa Fluor 647 goat antirabbit (Thermo Fisher Scientific), diluted in 3% BSA (1:250), at room temperature for 1 h. Filamentous actin was labeled with Alexa Fluor 568 phalloidin (Thermo Fisher Scientific) using a 1:250 dilution in 3% BSA. Nuclei were visualized with DAPI (Thermo Fisher Scientific) at 1:1000 in 3% BSA. Fluorescent imaging was performed using a Zeiss (LSM 880.

2.3.4. Histology and Immunohistochemistry. Vocal folds dissected from porcine larynxes were fixed in 4% PFA and paraffin-embedded for tissue sectioning at Histochemistry and Tissue Processing Core, Nemours. Samples (5 μm sections) were stained with Hematoxylin and Eosin (H&E) following standard protocols,[24] visualized on a Nikon (Tokyo, Japan) TS100-F phase contrast microscope, and imaged with a Nikon Coolpix camera. H&E stained cell nuclei purple and the surrounding matrix pink. Five-micrometer-thick sections were collected, deparaffinized at 55 °C, and antigen retrieved using a citrate buffer. Sections were permeabilized using PBST (0.025% tween) and blocked using 10% BSA for 45 min at room temperature. Samples were then incubated in solutions of primary antibodies (1:100 dilution in 3% BSA) overnight at 4 °C, followed by 1 h incubation in solutions of secondary antibodies (1:250 dilution in 3% BSA) at room temperature. Sections were

https://dx.doi.org/10.1021/acsbiomaterials.0c01741
ACS Biomater. Sci. Eng. XXXX, XXX, XXX–XXX

washed with PBS and counter stained for nuclei with DAPI (1:1000). Finally, mounting media (50% glycerol) was added with a coverslip and sections were imaged using a Zeiss LSM 880.

2.4. Statistical Analysis. All data are shown as a mean value with standard error of the mean from three technical repeats and three to four independent biological experiments. On the basis of the data set of each experiment, one-way analysis of variance (one-way ANOVA) or two-way analysis of variance (two-way ANOVA) was used for assessing significance levels for comparison of multiple groups. Unpaired two-tailed t test was used from comparison between two groups. A value of $p < 0.05$ was considered as statistically significant.

3. RESULTS

3.1. Characterization of Vocal Fold Tissues and Cells. Fresh porcine vocal fold tissues were obtained from animals subjected to experimental procedures that do not affect the larynx. We first characterized the porcine tissue by H&E staining to identify the distinct regions of vocal fold: the stratified squamous epithelium, the lamina propria and the muscle (Figure 1A). The thickness of the stratified epithelium was ~50 μm. Immunostaining (Figure 1B) shows the confinement of occludin to cell−cell junctions, indicating a tight epithelial barrier. The tissue exhibits a multilayered structure consisting of a basal layer and 4−5 suprabasal layers. As key components of intermediate filaments, KRT13 was detected throughout the epithelial strata (Figure 1C), whereas KRT14 expression was confined to the basal layer (Figure 1D). Similar observations with spatial localization of KRT13 and 14 have been observed in human vocal fold epithelium.[25]

Primary VFECs and VFFs were released from the tissue via enzymatic digestion. We modified the established protocol[14] to obtain pure populations of VFECs and VFFs. Our method relies on differential adhesion of VFFs and VFECs to coated and uncoated plates.[15,26−28] Cells isolated from the epithelium tissue were allowed to grow into confluence and trypsinized. When replated on a flask without a collagen IV coating, VFFs readily attached, allowing collection of the nonadherent, floating population of cells that were primarily VFECs. These cells were replated on collagen IV-coated flasks for expansion of a pure population of epithelial cells. The attached VFFs were cultured in fibroblast growth media to obtain a pure population of fibroblasts. This step is essential, as VFECs are sensitive to culture conditions; slight changes in isolation protocol, seeding density, and subculture method led to compromised viability. Moreover, adventitious VFFs proliferated rapidly, suppressed VFEC proliferation, and dominated the culture.

VFECs adopted a cobblestone morphology with close cell−cell contacts, whereas VFFs maintained a spindle-shaped morphology with elongated processes (Figure 2A). At passage 1, VFECs exhibited a doubling time of 37 h (Figure 2B). As the number of passages increased, the growth rate decreased, reaching a doubling time of 60 h by passage 6. Contrarily, VFFs continued to divide every 25 h even at higher passages. Overall, VFECs proliferated more slowly compared to VFFs, in agreement with a previous report.[14] Thus, VFECs were used in subsequent experiments up to passage 3, whereas VFFs were used between passages 1 and 6.

The purity of each cell type was confirmed by flow cytometry using CD90 as a fibroblast marker and cytokeratins 14, 15, 16, and 19 (KRT) as the epithelial marker (Figure 3A). Here, the relative expression level of CD90 and KRT is calculated on the basis of low/high gating on a single-marker analysis. In agreement with prior literature, although both cell

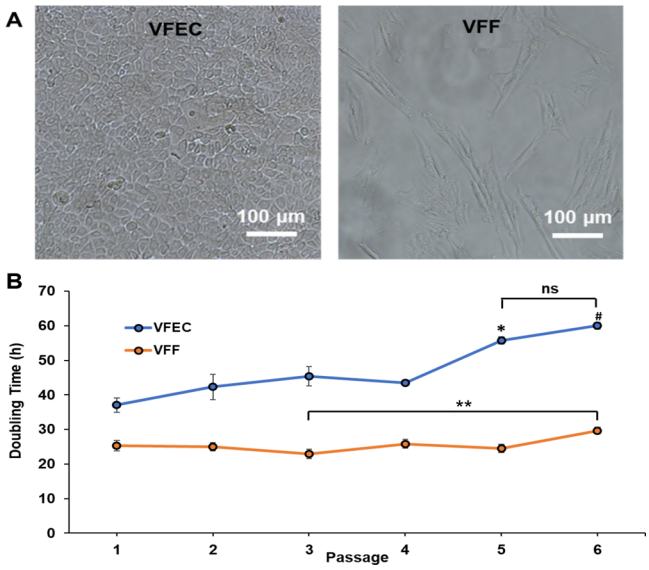

Figure 2. Morphology and growth kinetics of primary porcine VFECs and VFFs. (A) Phase contrast images of freshly isolated VFECs and VFFs grown on tissue culture plates. (B) Growth kinetics for VFECs and VFFs, in terms of doubling time as a function of passage number. */#: Significantly different compared to passages 1−4 for VFECs. ns: Not significantly different between passages 5 and 6 for VFECs. **: Significantly different between passages 3 and 6 for VFFs ($p < 0.05$, ANOVA, post hoc Tukey).

types expressed KRT and CD90,[15] a significantly ($p < 0.05$) higher level of KRT was detected in culture-expanded VFECs, whereas a significantly ($p < 0.05$) higher level of CD90 was detected in VFFs. The distribution of each cell population was further analyzed by double staining, and our results show that VFEC isolation was 70% KRT+ and VFFs were 78% CD90+ (Figure 3B). Of note, approximately 30% of VFECs and 22% of VFFs were positive for both markers.

Culture-expanded cells were further characterized by immunofluorescence (Figure 4). Confluent VFEC cultures were composed entirely of polygonally shaped cells free of contamination from fibroblasts. Confluent VFF cultures were also morphologically pure, and cells were entirely spindle shaped with elongated processes. Isolated VFECs were stained positive for KRT13 and showed distinct paracellular localization of both anchoring and tight junction markers E-cadherin, occludin, and ZO-1. On the other hand, VFFs were stained negative for KRT13 or tight junction markers. Expression of classical mesenchymal marker, vimentin, confirmed the mesenchymal phenotype. Cells developed aligned F-actin stress fibers traversing the entire cell body. In summary, our method of isolation yielded a pure population of VFECs expressing epithelial markers, tight junction, and anchoring junction markers similar to the native tissue.

3.2. Characterization of synthetic matrices. Hydrogels with varying HA concentrations (HA10 and HA24) were fabricated using HA-SH and HA-AES (Figure 5A). Because sulfhydryl groups were stoichiometrically in excess relative to the acrylate groups (18 and 4 molar excess for HA10 and HA24, respectively), both thiol−acrylate and thiol−thiol reactions contribute to the overall bulk mechanics.[22] By oscillatory shear rheometry (Figure 5B), HA10 and HA24 exhibit an elastic modulus (G') of 41.0 ± 7.0 and 1828.4 ± 180.3 Pa, respectively. Both gels were viscoelastic, having a loss modulus (G'') of 0.5 ± 0.2 and 5.4 ± 0.6 Pa, respectively.

https://dx.doi.org/10.1021/acsbiomaterials.0c01741
ACS Biomater. Sci. Eng. XXXX, XXX, XXX−XXX

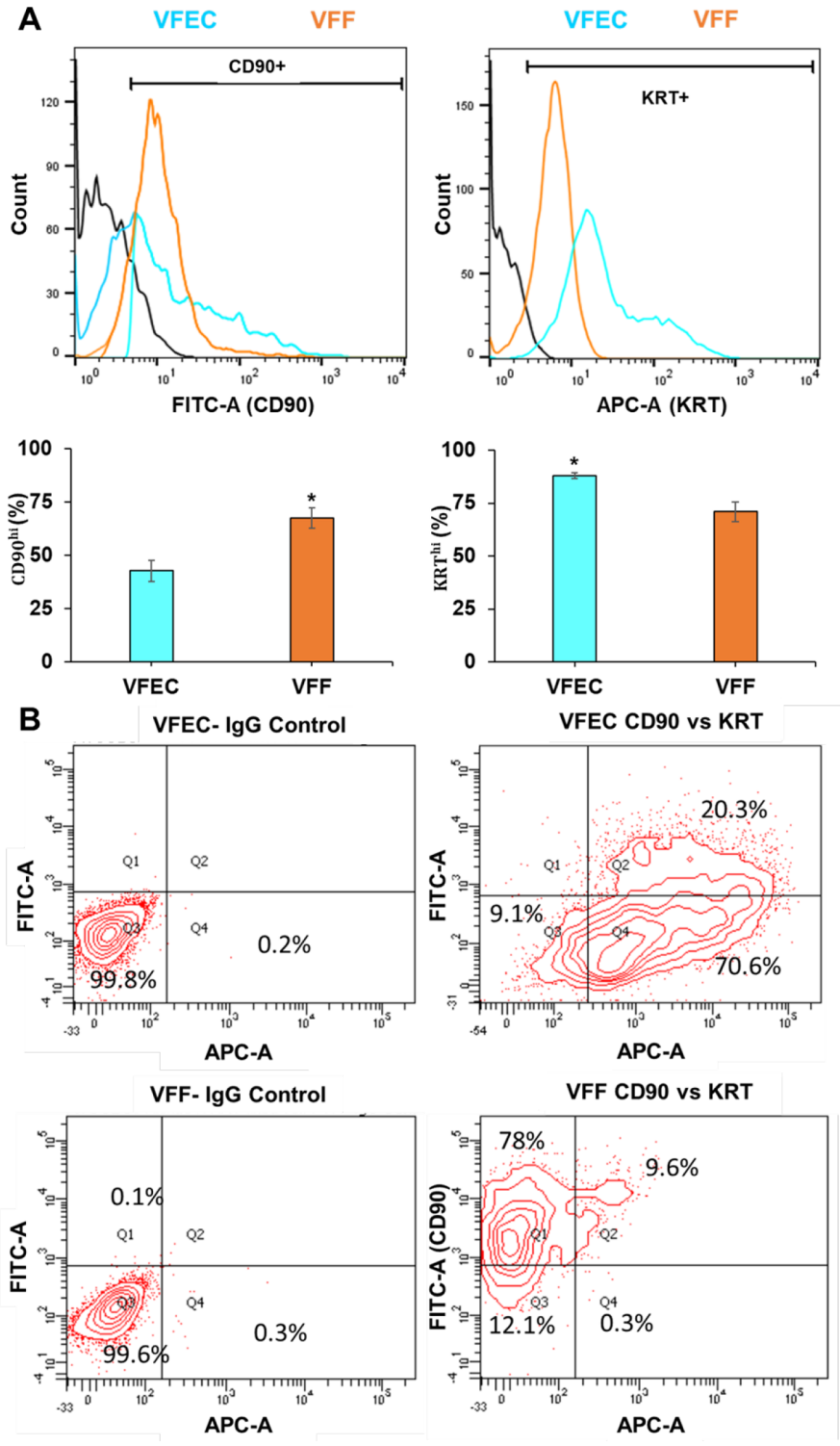

Figure 3. Flow cytometry analysis of primary porcine VFECs and VFFs. (A) Expression of CD90 and KRT in VFF and VFEC at P3. Fluorescence expression of FITC-CD90 and Alexa 647 KRT represented with low/high gates are shown in black. Percent positive cells was calculated based on the distribution of expression on the histogram. Data are means ± SEM (n = 4). *: Significantly different (p = 0.023 for CD90 expression in VFFs and 0.011 for KRT expression in VFECs, Student t test). (B) Representative CD90/KRT double staining contour plots for VFEC and VFF, along with their respective IgG controls.

To promote cell attachment and proliferation, we immobilized fibronectin-derived integrin binding peptide (RGDSP)[29,30] and laminin-derived syndecan-1-binding peptide (AG73)[31,32] on the hydrogel via rapid and efficient thiol-maleimide reaction. In our procedure, an equal volume of the peptide solution containing the same concentration of each peptide was introduced 5 min after HA-SH and HA-AES had been mixed to promote surface immobilization of peptide epitopes, although peptide conjugation in the bulk cannot be ruled out. Standard HPLC methods[33] were employed to

https://dx.doi.org/10.1021/acsbiomaterials.0c01741
ACS Biomater. Sci. Eng. XXXX, XXX, XXX−XXX

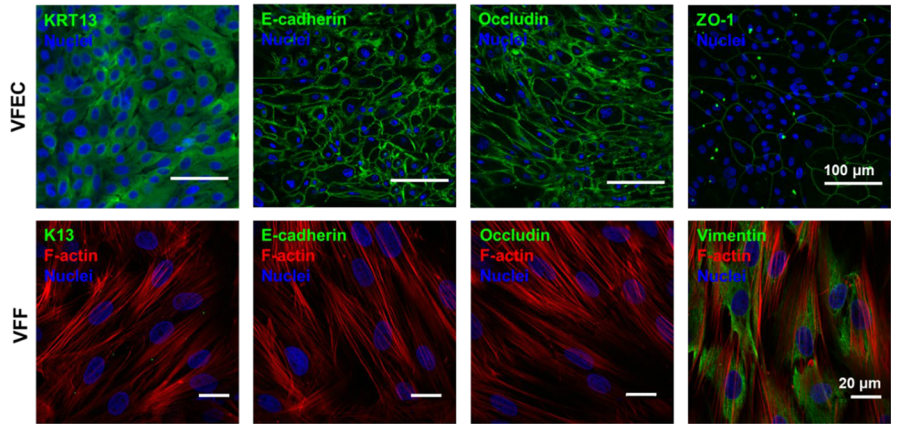

Figure 4. Phenotypic characterization of primary porcine VFECs and VFFs by immunofluorescence. VFECs were stained positive for stratified epithelial marker KRT13 and anchoring and tight junction markers E-cadherin, occludin, and ZO-1. VFFs were stained negative for KRT13, E-cadherin, and occludin, but positive for vimentin, a classical mesenchymal marker.

quantify the peptide concentration in the recovered supernatant and wash solutions after 30 min of a cross-linking/conjugation reaction. Our results (Figure 5C) show greater than 97% peptide conjugation under all conditions. For HA24, there was significantly ($p < 0.05$) more unconjugated AG73-MI (2.91 ± 0.23%) than RGDSP-MI (0.79 ± 0.12%). For HA10, similar amounts of AG73-MI (2.27 ± 0.16%) and RGDSP-MI (1.12 ± 0.43%) were detected from the combined supernatant and wash solutions. Importantly, comparison of the same peptide conjugated to different substrates did not reveal any statistical significance ($p > 0.05$). Collectively, these results indicate that the peptides were quantitatively incorporated to HA gels at similar levels between HA24 and HA10.

3.3. Development of Hydrogel-Supported Epithelium. Using HA-derived hydrogels, we established an *in vitro* cultivation procedure (Figure 6) for the establishment of engineered vocal fold epithelium. First, we evaluated the effects of peptide signals and substrate stiffness on VFEC attachment and proliferation (Figure 7). Cell−matrix interactions were analyzed based on the percentage of calcein positive area from Live/Dead confocal images. Minimal cell attachment was observed on HA gels without any peptide signals by day 7. When presented alone, RGDSP or AG73 enhanced cell attachment, but cells remain individually anchored. No significant difference was observed between soft and stiff hydrogels. Combination of RGDSP and AG73 signals led to significant enhancement of cell attachment with the formation of cell colonies only on HA24, but not HA10. When cultures were extended to day 14, no significant cell proliferation was observed on HA10 or HA24 with AG73 alone. Small cell colonies were detected on HA10 with RGDSP or RGDSP/AG73, but the surface coverage remained low (<20%). Significantly larger colonies were developed on HA24 with RGD or RGDSP/AG73. Compared to gels with RGDSP alone, HA24 with both RGDSP and AG73 signals led to the formation of a large cell sheet with >90% surface coverage. By day 21, only HA24 presenting both AG73/RGDSP promoted the development of a confluent monolayer (Figure S3).

Next, VFEC cultures on HA hydrogels were continued at the air−liquid interface to promote stratification. Live/Dead staining (Figure 8A) shows that, by day 42, a few isolated cells were detected on AG73-decorated HA10 gels. Significantly more cells were attached to AG73-decorated HA24 gels, but cells lost epithelial morphology and became elongated. Small colonies of cells on RGDSP-containing HA10 coalesced into larger islands, and those on RGDSP-presenting HA24 gels formed a large sheet on top of a closely packed cell layer. Cells on HA24 gels with both AG73/RGDSP signals were completely covered by layers of cells. Although cell morphology varied from top to bottom, cell−cell proximity was still maintained. When presented on HA10 gels, the combined peptide signals led to formation of patchy cell sheets without stratification.

Cultures were further stained for F-actin to assess cell morphology. As shown in Figure 8B, cells on HA24 under RGDSP or RGDSP/AG73 conditions were cuboidal shaped with cortical F-actin organized at cell−cell junctions. On HA24 with AG73, VFECs had partially differentiated to nonepithelial cells with F-actin stress fibers traversing the entire cell body. On HA10, regardless of peptide identity, VFECs completely lost their cobblestone morphology and adopted fibroblast-like phenotype as evidenced by the presence of cytoskeletal stress fibers. Cells cultured on HA10, regardless of the peptides, do not display robust staining of KRT13. Cells on HA24 with RGDSP or RGDSP/AG73 were stained consistently and uniformly for KRT13 throughout the cell layer. On AG73-decorated HA24, KRT13+ cells coexisted with fibroblast-like cells. 3D rendering of the z-stacks of structures developed on gels presenting both AG73/RGDSP signals shows a uniform monolayer on HA24 compared to HA10, where incomplete surface coverage was observed (Figure S4). The cross-sectional view of these hydrogels showed that there was an incomplete cellular monolayer on HA10, whereas HA24 had two disorganized cell layers (Figure 8B).

Our results show that HA24 with both RGDSP and AG73 is most conducive to the development of stratified epithelium. Compared to the native tissue, however, the engineered tissue in thinner and less organized. Thus, biochemical and biomechanical signals from the matrix alone are not sufficient for stratification of VFECs. Studies have highlighted the importance of cytokine signals from the underlying stromal tissue in promoting stratification of epithelial cells.[34−36] Here, we used VFF-conditioned media to regulate the stratification of VFECs on HA24 gel presenting both AG73/RGDSP peptide signals. Replacing the FAD media with VFF-conditioned DMEM growth media on day 14 resulted in further stratification of VFECs. As shown in Figure 9, the

https://dx.doi.org/10.1021/acsbiomaterials.0c01741
ACS Biomater. Sci. Eng. XXXX, XXX, XXX−XXX

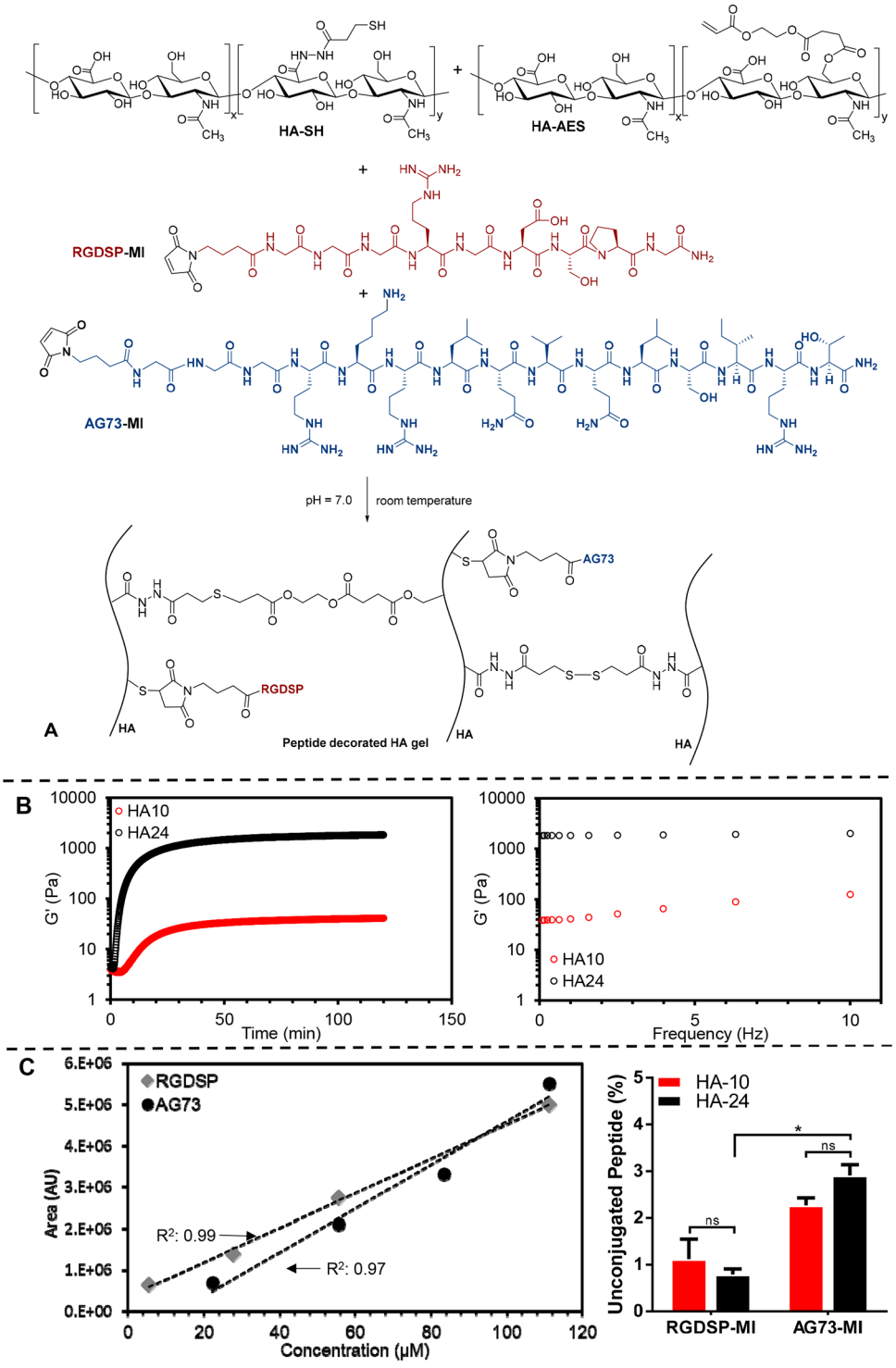

Figure 5. Synthesis and characterization of bioactive HA hydrogels. (A) Hydrogel was derived from HA-SH, HA-AES, RGDSP-MI, and AG73-MI. (B) Rheological characterization of HA hydrogels. Left: time sweep; right, frequency sweep. (C) HPLC characterization of peptide conjugation. Left: standard curves constructed from integrated peak areas for RGDSP-MI and AG73-MI. Solid symbol - raw data; dotted line - linear fit. Right: percent unconjugated peptide as a function of peptide identity and hydrogel composition. *: Significant difference between the indicated groups, ($p < 0.05$, two-way ANOVA, post hoc Tukey).

engineered epithelium contained 4−5 cell layers. Cells expressed KRT13, E-cadherin, MUC1, and occludin throughout the strata. Involucrin was expressed in the superficial and middle layers, but not the basal layer, consistent with what is observed in human tissues.[25] Integrin β1 was more concentrated in the basal layer indicating stronger cell−substrate interactions. Collagen IV and laminin 5 were detected beneath the basal cells. The engineered epithelium is morphologically similar to the native tissue (Figure 10), although the latter contained one additional cell layer. Both tissues exhibit homogeneous distribution of KRT13 throughout the strata and proliferative basal cells stained positive for

https://dx.doi.org/10.1021/acsbiomaterials.0c01741
ACS Biomater. Sci. Eng. XXXX, XXX, XXX−XXX

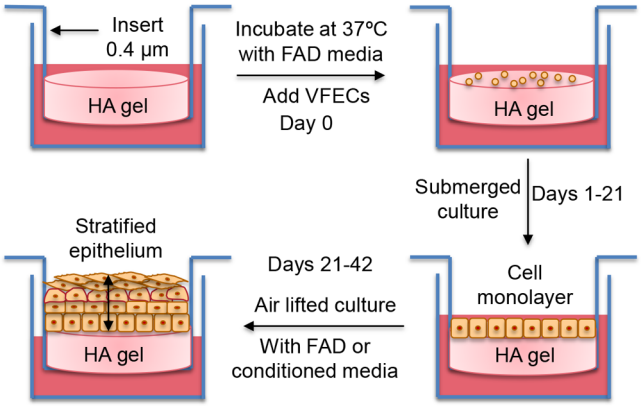

Figure 6. Experimental procedure for the establishment of stratified epithelium.

Ki67. The positive staining for tight junction and anchoring junction markers (E-cadherin and occludin) and basement membrane proteins (collagen IV and laminin 5) indicates an intact epithelium. These observations confirmed that cytokine signals from the fibroblasts are necessary for stratification of VFECs.

4. DISCUSSION

Vocal fold epithelium is a multilayered tissue with distinct cellular organizations[25,37] similar to that covering the cornea,[35,38] vagina,[39] oral cavity, and esophagus.[40] Held together by tight and adherent junctions,[41] the epithelium serves as a protective barrier, controls solute diffusion, and maintains tissue homeostasis.[42,43] Our strategy for the establishment of a vocal fold epithelium model relies on the availability of pure primary cells. Literature reports on *in vitro* culture of VFECs are sparse; these cells were isolated from humans,[15,44] rabbits,[13] and pigs.[14] Primary human VFEC cultures are not feasible because of the inaccessibility of the tissue, its susceptibility to surgical damage, and the scarcity of healthy human tissues. A porcine model was chosen for the current study because of the morphological and functional similarities of porcine vocal fold epithelium to that of humans, and the availability and abundance of healthy porcine tissues. One of the main challenges associated with the expansion and stratification of primary epithelial culture is the requirement of feeder (e.g., murine 3T3 fibroblasts[13]) or supporting cells (e.g., VFFs[15]). A recent study has shown successful culture of porcine VFEC without feeder cells in FAD media. However, under the experimental conditions employed, only cell monolayer was developed.[14]

Our cell isolation protocol yielded relatively pure epithelial and fibroblast cell populations. Previous work on cells isolated from human vocal fold tissues shows that, by single marker analysis, percent KRT+ cells in VFFs and VFECs was comparable and low, whereas percent CD90+ cells in VFFs is significantly higher than in VFECs. Our isolation resulted in VFEC population with higher percentage of KRT+ cells compared to CD90+ cells and VFF population with high percent of CD90+ cells compared to KRT+ cells. In both cases, the difference is significant. The double marker contour plot confirmed successful separation into $CD90^{hi}/KRT^{lo}$ VFFs and $CD90^{lo}/KRT^{hi}$ VFECs.

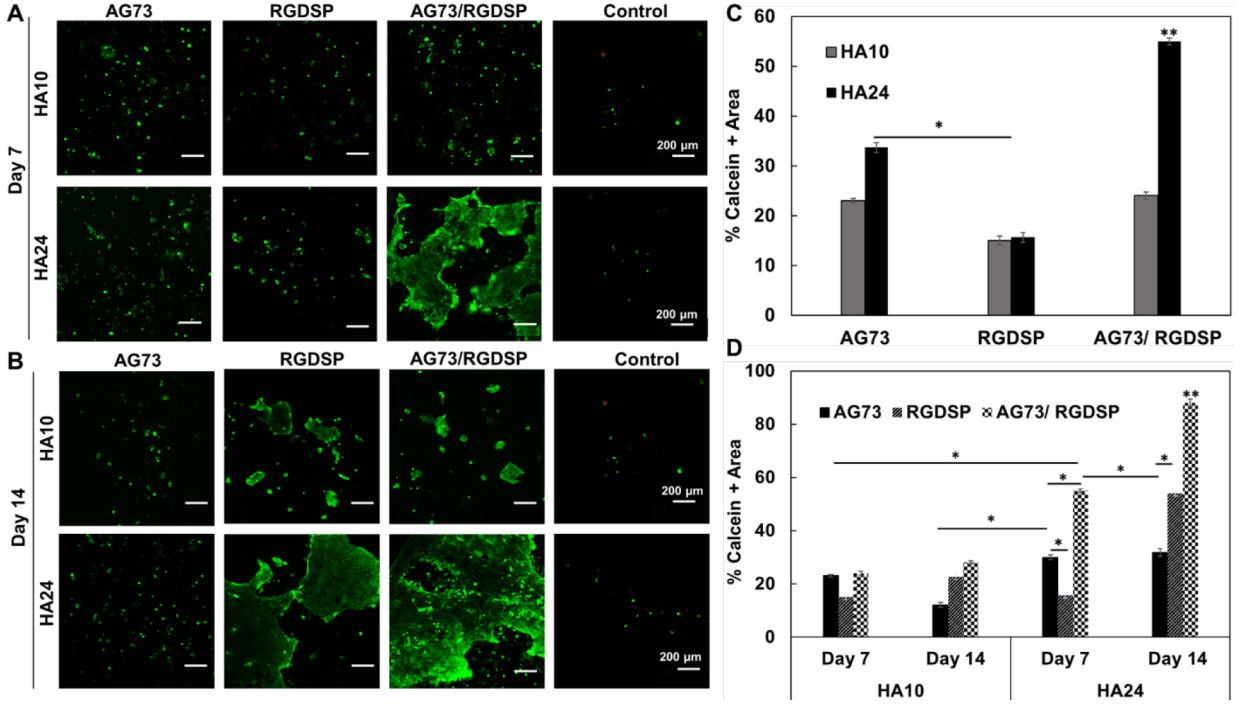

Figure 7. Effect of matrix composition and stiffness on VFEC attachment and proliferation under submerged culture conditions. (A, B) Confocal images of VFEC cultures after Live/Dead staining on day (A) 7 and (B) 14. Green: live cells; Red: dead cells. (C) Initial cell attachment on day 7, as percent calcein positive region, as a function of matrix composition. (D) Cell proliferation, as percent calcein positive regions on day 14 relative to day 7, as a function of matrix composition. Quantification was carried out using ImageJ software based on three separate 1024 × 1024 μm^2 confocal images. Error represents standard error of the mean of three repeats. **: Significant compared to all other groups. *: Significant difference between the indicated groups, ($p < 0.05$, ANOVA, post hoc Tukey).

https://dx.doi.org/10.1021/acsbiomaterials.0c01741
ACS Biomater. Sci. Eng. XXXX, XXX, XXX−XXX

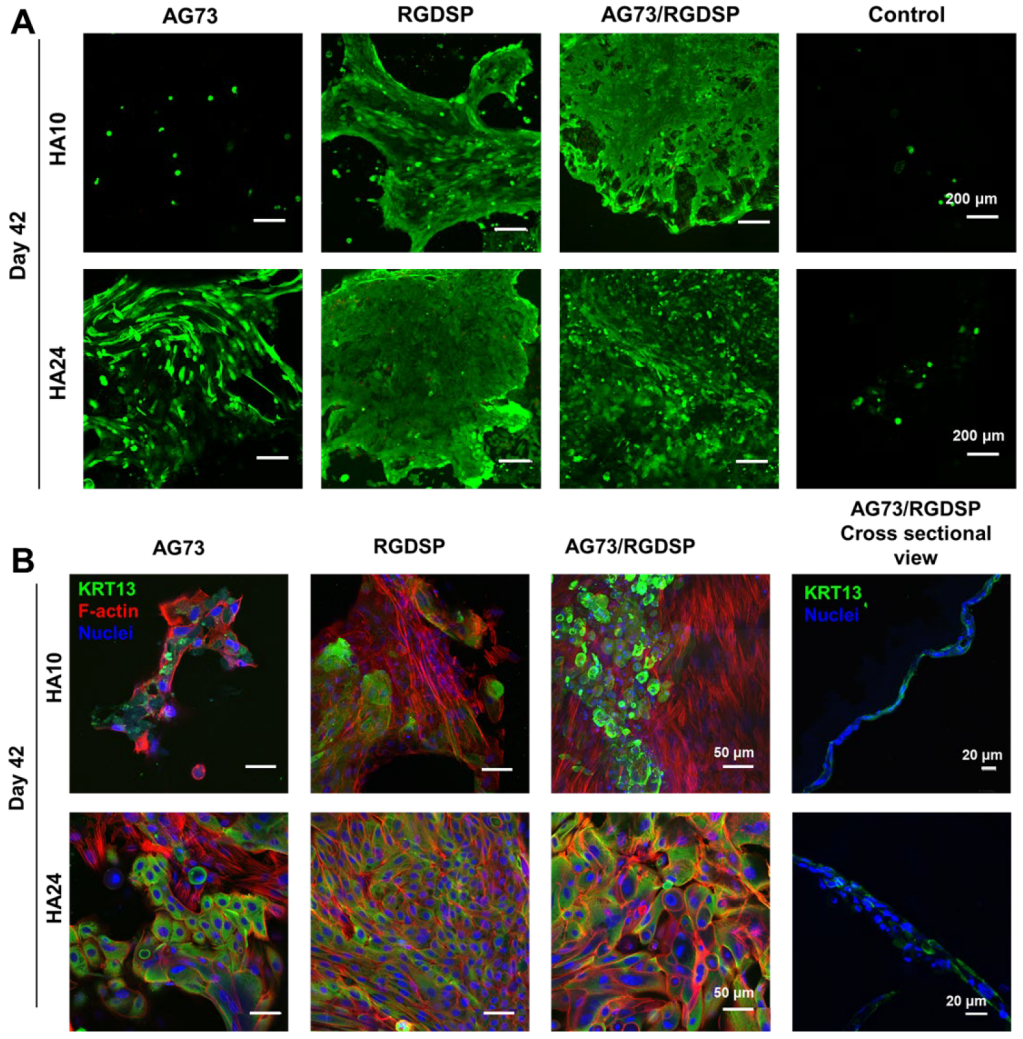

Figure 8. Effect of matrix composition and stiffness onVFEC stratification under air lifted culture conditions. (A) Confocal images of VFEC cultures on day 42 after Live/Dead staining. Green - live cells; Red - dead cells. (B) Representative confocal images of VFEC cultures on day 42 stained for KRT13 (green), F-actin (red), and nuclei (blue). HA10 down-regulated the expression of KRT13, suppressed the formation of cell−cell junctions and promoted the development F-actin stress fibers. HA24 with RGDSP and AG73/RGDSP maintained KRT13 expression and promoted the establishment of cell−cell junctions. In the presence of AG73/RGDSP, VFECs formed a monolayer on HA10, but stratified (2−3 layer of cells) on HA24.

Here, we report the first example of a hydrogel-supported stratified vocal fold epithelium without the cocultured fibroblast. HA-based hydrogels with immobilized bioactive peptides were developed to mimic the native tissue mechanically and compositionally. It is well accepted that substrate stiffness has a profound influence on adhesion, proliferation, and differentiation of cells of both mesenchymal and epithelial origins. In general, cells spread and proliferate more readily on stiff substrates, forming larger, stable, elongated focal adhesions and phosphorylate ERK in response to growth factor stimulation.[45,46] For stratified epithelial cells, physiologically relevant soft and compliant substrates promote higher proliferation and stratification, colony formation and the maintenance of stem/progenitor cell markers, whereas stiffer substrates promote differentiation.[47,48] Note, in the literature, soft substrates are physiologically relevant and stiff substrates often refer to nonphysiologic or pathological tissues. Here, both HA10 and HA24 are relatively soft.

The vocal fold epithelium is attached to a basement membrane that is anchored on the underlying connective tissue, lamina propria. Mechanically, the basement membrane couples the epithelium with the superfacial lamina propria to form a cohesive mucosa.[49] The pig vocal fold had a two-layer lamina propria, with the superfacial layer being mostly ground substance (HA), and the deep layer consisted mostly of collagen and elastin.[50,51] By torsional wave experiment, we have previously shown that adult tissues (the lamina propria and the epithelium combined) had an average storage modulus of 2309 ± 1394 Pa at frequencies of 36−200 Hz. The vocal folds of young pigs were significantly more compliant, with a storage modulus of 394 ± 142 Pa between 14 and 30 Hz. When analyzed by commercial rheometer at 0−10 Hz, tissues are significantly softer, from 220−1036 Pa at 0.016 Hz to 5976−8214 Pa at 10 Hz.[52] Thus, in terms of stiffness, HA24 matches the native tissue more closely than HA10.

Peptide-free HA substrates, regardless of the stiffness, do not support the attachment and growth of VFECs. Although mesenchymal cells or epithelial cells that have undergone mesenchymal transition can bind HA via the cell surface receptor, CD44 or RHAMM, healthy epithelial cells do not

https://dx.doi.org/10.1021/acsbiomaterials.0c01741
ACS Biomater. Sci. Eng. XXXX, XXX, XXX−XXX

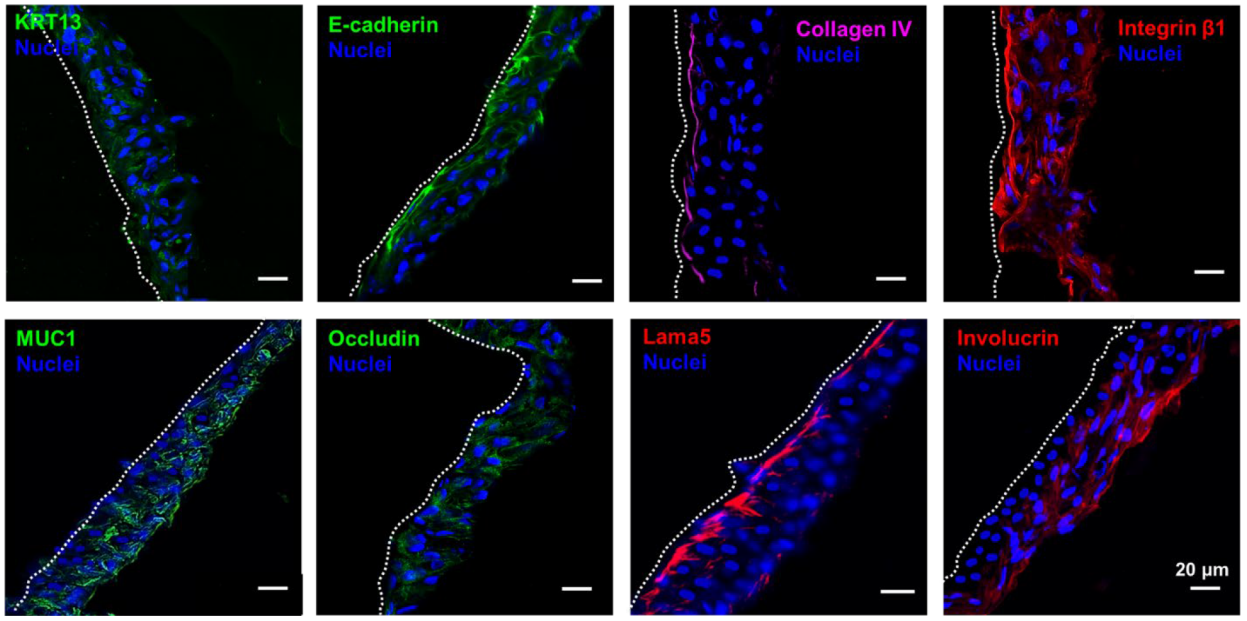

Figure 9. Characterization of stratified epithelium grown on HA24 with AG73 and RGDSP in the presence of VFF conditioned media. Cells expressed KRT13, E-cadherin, integrin β1, MUC1, and occludin throughout the strata. Collagen IV and Lama 5 were expressed by the basal cells, whereas involucrin+ cells were found in the suprabasal layers.

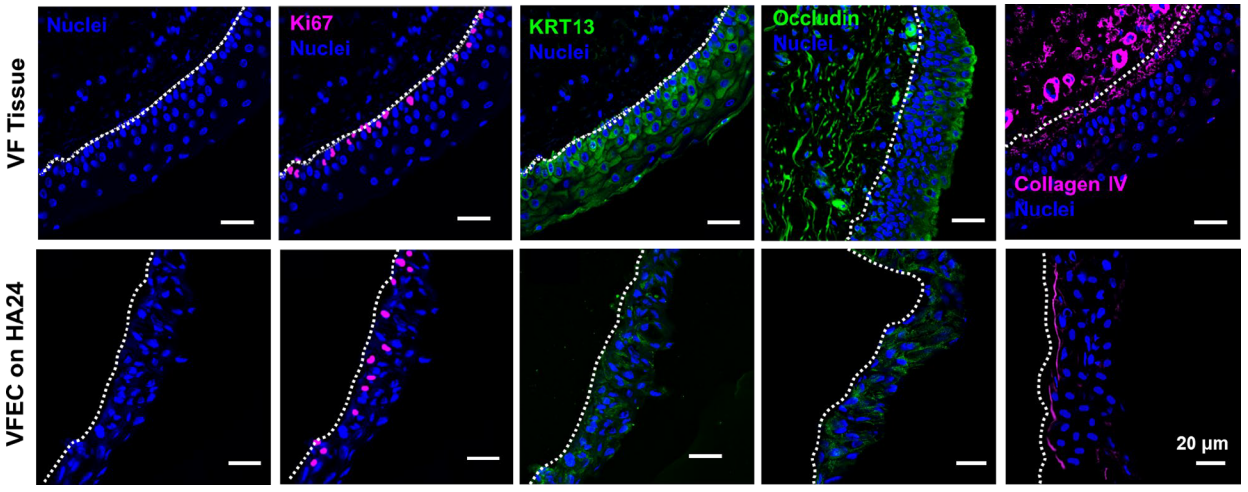

Figure 10. Comparison of engineered epithelium with the native tissue. The native tissue has 5−6 layers of stratified squamous epithelial cells (nuclei, blue), whereas the engineered tissue has 4−5 cell layers. Both native and engineered tissues exhibited a basal, proliferative cell layer, stained positive for Ki67 (pink). Both native and engineered tissues were stained positive for KRT13, occludin, and collagen IV, with similar staining patterns. The white dotted line delineates the tissue boundary (basement membrane).

express CD44 and are thus unable to interact with HA directly. Moreover, CD44-mediated cell adhesion is weak and dynamic, not sufficient to permanently anchor cells to a substrate.[53] Compositionally, the basement membrane is composed primarily of laminin, fibronectin, and collagen IV. Epithelial cells are known to bind fibronectin-derived RGDSP peptide through specific integrin receptors, such as $\alpha_6\beta_1$ and $\alpha_8\beta_1$.[54] Integrin-mediated cell−ECM interactions play a key role in establishing and maintaining association of cytoskeleton in neighboring cells through cadherins.[55,56]

As reported previously, syndecan-binding AG73 has been shown to promote the development of acini-like structures from salivary gland epithelial cells.[32] When conjugated to chitosan, AG73-promoted the attachment and proliferation of keratinocytes in vivo.[57] AG73 alone does not promote cell adhesion,[58] but when combined with integrin binding peptides, it synergistically accelerates cell adhesion and neurite outgrowth.[16,59]

Our work shows that the initial attachment and stratification of VFECs requires substrates with an optimal stiffness (1828 Pa) displaying both integrin and syndecan binding peptides. Our results further show that cells cultured on soft substrates (41 Pa) with RGDSP, alone or together with AG73, lost the cuboidal epithelial cell morphology and adopted mesenchymal-like morphology with elongated, F-actin-rich cell processes. Interestingly, a fraction of cells attached to HA24 with AG73 had also undergone morphological changes. VFF contamination is unlikely, as our isolation protocol resulted in relatively pure populations of VFFs and VFECs. Moreover, if VFFs were

https://dx.doi.org/10.1021/acsbiomaterials.0c01741
ACS Biomater. Sci. Eng. XXXX, XXX, XXX−XXX

present in our epithelial culture, they would appear under all culture conditions.

Epithelial cells exhibit cellular plasticity and dedifferentiation is often associated with tissue repair. For example, differentiated airway epithelial cells can revert into cells that are morphologically indistinguishable and functionally comparable to basal stem cells in repairing epithelial injury.[60] In the kidney during recovery from ischemia/reperfusion injury, surviving tubular epithelial cells dedifferentiate into cells with apparent stem cell markers; it is these dedifferentiated cells that are responsible for restoring tubular integrity.[61] Retinal pigment epithelium cells are also known to dedifferentiate in culture. When cultured on relatively soft substrates, these cells dedifferentiate into fibroblast-like cells, the mechanical environment was the dominating factor, and Activin A was unable to rescue these cells.[62]

In our case, all HA10-based substrates, as well as HA24 with AG73, do not promote the establishment of epithelial cell colonies with cell−cell contacts. These substrates failed to establish strong cellar adhesion through integrins. The surviving epithelial cells that do attach adapt to the loss of adjacent cells by dedifferentiating, possibly by degradation and/or relocalization of the junction proteins. On the other hand, VFECs cultured on HA24 with RGDSP/AG73 can generate large local substrate deformations that appeared to recruit adjacent epithelial cells into joining an evolving colony. Our study therefore highlights the importance of culturing VFECs on substrates with tissue-like stiffness and appropriate adhesive ligands to promote robust cell−matrix and subsequently cell−cell adhesion. These cells are primed to be responsive to exogenous factors from VFF-conditioned media to improve epithelium function.

Further stratification is achieved through paracrine signaling without the need for direct epithelial/fibroblast contacts using VFF-conditioned media. With 4−5 cell layers, the engineered tissue express tight junction marker occludin and adherens junction marker E-cadherin, confirming the stability of the tissue. The expression of MUC1 by the engineered tissue confirms the maintenance of VFECs function and the establishment of mucus barrier. Basal expression of Ki67 confirmed the regenerative capacity of VFECs. Cellular deposition of basement membrane proteins laminin 5 and collagen IV suggests the establishment of barrier function. The positive staining in the luminal cell layers for involucrin, a protein to be expressed at the surface of stratified squamous epithelium, including the vocal fold and the epidermis,[25] further confirm successful stratification.

Earlier work on epithelial stem cells of the thymus and epidermis, cytokine signals from the underlying stromal tissue, and expression of p63 is important for stratification of epithelial cells.[34−36] A number of studies have identified cytokine signals contributing to the stratification of epithelial cells. For example, it has been reported that fibroblast growth factor-7 (FGF-7) is essential for bladder urothelial stratification,[63] FGF-10 is required for stratification of vaginal epithelium.[64] Transforming growth factor beta (TGF-β1) regulates the esophageal epithelial barrier,[65] and bone morphogenetic protein (BMP7) signaling is required for stratification of mouse esophageal epithelium cells.[66] Identification of specific cytokines conductive to VFEC stratification will allow for the establishment of engineered vocal fold epithelium under defined conditions using appropriate factors at appropriate concentrations. This is the subject of our current investigation.

5. CONCLUSION

Toward the goal of establishing an *in vitro* model of vocal fold cover, we isolated primary porcine VFECs and purified and expanded them in culture. HA-based hydrogels recapitulating the biochemical composition of the basement membrane and the biomechanical properties of the underlying lamina propria were prepared using thiolated HA, acrylated HA, and maleimide-functionalized integrin- and syndecan-binding peptides. VFECs attached and proliferated on HA gels that exhibited an elastic shear modulus of 1828 Pa and contained both RGDSP and AG73, but not on gels with a G' of 40 Pa or with only RGDSP or AG73 peptide. Following a 21-day submerged culture and 21-day air-lifted culture, a trilayered epithelium with proliferating cells was developed. Culture of VFECs in VFF-conditioned media led to more robust stratification; the epithelium consisted of 4−5 distinct cell layers, expressing Ki67, collagen IV, and laminin 5 at the basal layer and KRT13, E-cadherin, and occludin throughout the epithelial strata. This work highlights the importance of matrix properties, cytokine signaling, and cell−cell communication in VFEC function, in terms of attachment, proliferation, and stratification.

■ ASSOCIATED CONTENT

Supporting Information

The Supporting Information is available free of charge at https://pubs.acs.org/doi/10.1021/acsbiomaterials.0c01741.

Antibody information, characterization of peptides by ESI-MS and HPLC, and confocal images of hydrogel-supported epithelium (PDF)

■ AUTHOR INFORMATION

Corresponding Author

Xinqiao Jia − *Department of Materials Science and Engineering, Department of Biological Sciences, Department of Biomedical Engineering, and Delaware Biotechnology Institute, University of Delaware, Newark, Delaware 19716, United States;* orcid.org/0000-0002-3564-5576; Phone: 302-831-6553; Email: xjia@udel.edu; Fax: 302-831-4545

Authors

Anitha Ravikrishnan − *Department of Materials Science and Engineering, University of Delaware, Newark, Delaware 19716, United States;* orcid.org/0000-0002-2385-563X

Eric W. Fowler − *Department of Materials Science and Engineering, University of Delaware, Newark, Delaware 19716, United States;* orcid.org/0000-0002-2640-8915

Alexander J. Stuffer − *Department of Biological Sciences, University of Delaware, Newark, Delaware 19716, United States*

Complete contact information is available at: https://pubs.acs.org/10.1021/acsbiomaterials.0c01741

Author Contributions

†A.R. and E.W.F. contributed equally to this work.

Notes

The authors declare no competing financial interest.

https://dx.doi.org/10.1021/acsbiomaterials.0c01741
ACS Biomater. Sci. Eng. XXXX, XXX, XXX−XXX

■ ACKNOWLEDGMENTS

This work was supported in part by National Institutes of Health (NIDCD, R01DC014461), National Science Foundation (NSF, DMR 1809612), and Delaware Bioscience Center. Instrumentation was supported by NIH grants P30GM110758, P20GM104316, S10RR026962, and S10OD016267 and NSF grants CHE-0840401, CHE-1229234, and CHE-1048367. We thank Dr. Robert Mauck for providing porcine tissues, Dr. Jeffrey Caplan for his advice on confocal imaging, Chen-Yuan Kaofor his guidance on flow cytometry, and Terry Kokas for assistance with tissue embedding and sectioning. We acknowledge Sanofi/Genzyme for providing HA.

■ REFERENCES

(1) Gray, S. D. Cellular Physiology of the Vocal Folds. *Otolaryngol Clin North Am.* **2000**, *33* (4), 679−698.
(2) Chen, X.; Thibeault, S. L. Characteristics of age-related changes in cultured human vocal fold fibroblasts. *Laryngoscope* **2008**, *118* (9), 1700−4.
(3) Jetté, M. E.; Hayer, S. D.; Thibeault, S. L. Characterization of human vocal fold fibroblasts derived from chronic scar. *Laryngoscope* **2013**, *123* (3), 738−45.
(4) Leydon, C.; Imaizumi, M.; Yang, D.; Thibeault, S. L.; Fried, M. P. Structural and functional vocal fold epithelial integrity following injury. *Laryngoscope* **2014**, *124* (12), 2764−9.
(5) Levendoski, E. E.; Leydon, C.; Thibeault, S. L. Vocal fold epithelial barrier in health and injury: a research review. *Journal of speech, language, and hearing research: JSLHR* **2014**, *57* (5), 1679−91.
(6) Kojima, T.; Van Deusen, M.; Jerome, W. G.; Garrett, C. G.; Sivasankar, M. P.; Novaleski, C. K.; Rousseau, B. Quantification of acute vocal fold epithelial surface damage with increasing time and magnitude doses of vibration exposure. *PLoS One* **2014**, *9* (3), No. e91615.
(7) Kojima, T.; Valenzuela, C. V.; Novaleski, C. K.; Van Deusen, M.; Mitchell, J. R.; Garrett, C. G.; Sivasankar, M. P.; Rousseau, B. Effects of phonation time and magnitude dose on vocal fold epithelial genes, barrier integrity, and function. *Laryngoscope* **2014**, *124* (12), 2770−8.
(8) Hirano, S. Current Treatment of Vocal Fold Scarring. *Curr. Opin Otolaryngol Head Neck Surg.* **2005**, *13* (3), 143−147.
(9) Leydon, C.; Imaizumi, M.; Bartlett, R. S.; Wang, S. F.; Thibeault, S. L. Epithelial Cells are Active Participants in Vocal Fold Wound Healing: An in vivo Animal Model of Injury. *PLoS One* **2014**, *9* (12), No. e115389.
(10) Novaleski, C. K.; Carter, B. D.; Sivasankar, M. P.; Ridner, S. H.; Dietrich, M. S.; Rousseau, B. Apoptosis and Vocal Fold Disease: Clinically Relevant Implications of Epithelial Cell Death. *J. Speech Lang Hear Res.* **2017**, *60* (5), 1264−1272.
(11) Leydon, C.; Imaizumi, M.; Yang, D.; Thibeault, S. L.; Fried, M. P. Structural and Functional Vocal Fold Epithelial Integrity Following Injury. *Laryngoscope* **2014**, *124* (12), 2764−2769.
(12) Sakai, N.; Tager, A. M. Fibrosis of Two: Epithelial Cell-Fibroblast Interactions in Pulmonary Fibrosis. *Biochim. Biophys. Acta, Mol. Basis Dis.* **2013**, *1832* (7), 911−921.
(13) Mizuta, M.; Kurita, T.; Kimball, E. E.; Rousseau, B. Structurally and Functionally Characterized in vitro Model of Rabbit Vocal Fold Epithelium. *Tissue Cell* **2017**, *49* (3), 427−434.
(14) Erickson-DiRenzo, E.; Leydon, C.; Thibeault, S. L. Methodology for the Establishment of Primary Porcine Vocal Fold Epithelial Cell Cultures. *Laryngoscope* **2019**, *129* (10), E355−E364.
(15) Ling, C.; Li, Q.; Brown, M. E.; Kishimoto, Y.; Toya, Y.; Devine, E. E.; Choi, K. O.; Nishimoto, K.; Norman, I. G.; Tsegyal, T.; Jiang, J. J.; Burlingham, W. J.; Gunasekaran, S.; Smith, L. M.; Frey, B. L.; Welham, N. V. Bioengineered Vocal Fold Mucosa for Voice Restoration. *Sci. Transl. Med.* **2015**, *7* (314), 314ra187.
(16) Weeks, B. S.; Nomizu, M.; Ramchandran, R. S.; Yamada, Y.; Kleinman, H. K. Laminin-1 and the RKRLQVQLSIRT Laminin-1 α1 Globular Domain Peptide Stimulate Matrix Metalloproteinase Secretion by PC12 Cells. *Exp. Cell Res.* **1998**, *243* (2), 375−382.
(17) Chan, R. W.; Gray, S. D.; Titze, I. R. The Importance of Hyaluronic Acid in Vocal Fold Biomechanics. *Otolaryngol.–Head Neck Surg.* **2001**, *124* (6), 607−614.
(18) Butler, J. E.; Hammond, T. H.; Gray, S. D. Gender-related Differences of Hyaluronic Acid Distribution in the Human Vocal Fold. *Laryngoscope* **2001**, *111* (5), 907−911.
(19) Dicker, K. T.; Gurski, L. A.; Pradhan-Bhatt, S.; Witt, R. L.; Farach-Carson, M. C.; Jia, X. Hyaluronan: A Simple Polysaccharide with Diverse Biological Functions. *Acta Biomater.* **2014**, *10* (4), 1558−1570.
(20) Turley, E. A.; Noble, P. W.; Bourguignon, L. Y. Signaling Properties of Hyaluronan Receptors. *J. Biol. Chem.* **2002**, *277* (7), 4589−4592.
(21) Jiang, D.; Liang, J.; Noble, P. W. Hyaluronan in Tissue Injury and Repair. *Annu. Rev. Cell Dev. Biol.* **2007**, *23*, 435−461.
(22) Ozdemir, T.; Fowler, E. W.; Liu, S.; Harrington, D. A.; Witt, R. L.; Farach-Carson, M. C.; Pradhan-Bhatt, S.; Jia, X. Tuning Hydrogel Properties to Promote the Assembly of Salivary Gland Spheroids in 3D. *ACS Biomater. Sci. Eng.* **2016**, *2* (12), 2217−2230.
(23) Zerdoum, A. B.; Fowler, E. W.; Jia, X. Induction of Fibrogenic Phenotype in Human Mesenchymal Stem Cells by Connective Tissue Growth Factor in a Hydrogel Model of Soft Connective Tissue. *ACS Biomater. Sci. Eng.* **2019**, *5* (9), 4531−4541.
(24) Suvarna, S. K.; Layton, C.; Bancroft, J. D. *Theory and Practice of Histology Techniques*, 8th ed.; Elsevier: 2019.
(25) Dowdall, J. R.; Sadow, P. M.; Hartnick, C.; Vinarsky, V.; Mou, H.; Zhao, R.; Song, P. C.; Franco, R. A.; Rajagopal, J. Identification of Distinct Layers within the Stratified Squamous Epithelium of the Adult Human True Vocal Fold. *Laryngoscope* **2015**, *125* (9), E313−E319.
(26) Rouger, K.; Fornasari, B.; Armengol, V.; Jouvion, G.; Leroux, I.; Dubreil, L.; Feron, M.; Guevel, L.; Cherel, Y. Progenitor Cell Isolation from Muscle-derived Cells based on Adhesion Properties. *J. Histochem. Cytochem.* **2007**, *55* (6), 607−618.
(27) Riva, F.; Casasco, A.; Casasco, M.; Calligaro, A.; Cornaglia, A. I., Growth and Stratification of Epithelial Cells in Minimal Culture Conditions. In *Epidermal Cells*; Methods in Molecular Biology; Humana Press: Totowa, NJ, 2010; Vol. *585*, pp 25−43.
(28) Ilmarinen, T.; Laine, J.; Juuti-Uusitalo, K.; Numminen, J.; Seppänen-Suuronen, R.; Uusitalo, H.; Skottman, H. Towards a Defined, Serum-and Feeder-free Culture of Stratified Human Oral Mucosal Epithelium for Ocular Surface Reconstruction. *Acta Ophthalmol.* **2013**, *91* (8), 744−750.
(29) Peppas, N.; Huang, Y.; Torres-Lugo, M.; Ward, J.; Zhang, J. Physicochemical Foundations and Structural Design of Hydrogels in Medicine and Biology. *Annu. Rev. Biomed. Eng.* **2000**, *2* (1), 9−29.
(30) Ruoslahti, E. RGD and Other Recognition Sequences for Integrins. *Annu. Rev. Cell Dev. Biol.* **1996**, *12* (1), 697−715.
(31) Hoffman, M. P.; Engbring, J. A.; Nielsen, P. K.; Vargas, J.; Steinberg, Z.; Karmand, A. J.; Nomizu, M.; Yamada, Y.; Kleinman, H. K. Cell type-specific Differences in Glycosaminoglycans Modulate the Biological Activity of a Heparin-binding Peptide (RKRLQVQLSIRT) from the G Domain of the Laminin α1 Chain. *J. Biol. Chem.* **2001**, *276* (25), 22077−22085.
(32) Hoffman, M. P.; Nomizu, M.; Roque, E.; Lee, S.; Jung, D. W.; Yamada, Y.; Kleinman, H. K. Laminin-1 and Laminin-2 G-Domain Synthetic Peptides Bind Syndecan-1 and are Involved in Acinar Formation of a Human Submandibular Gland Cell Line. *J. Biol. Chem.* **1998**, *273* (44), 28633−28641.
(33) Lough, W. J.; Wainer, I. W. *High Performance Liquid Chromatography: Fundamental Principles and Practice*; Springer: 1995.
(34) Senoo, M.; Pinto, F.; Crum, C. P.; McKeon, F. p63 is Essential for the Proliferative Potential of Stem Cells in Stratified Epithelia. *Cell* **2007**, *129* (3), 523−536.
(35) Koizumi, N.; Inatomi, T.; Suzuki, T.; Sotozono, C.; Kinoshita, S. Cultivated Corneal Epithelial Stem Cell Transplantation in Ocular Surface Disorders. *Ophthalmology* **2001**, *108* (9), 1569−1574.

https://dx.doi.org/10.1021/acsbiomaterials.0c01741
ACS Biomater. Sci. Eng. XXXX, XXX, XXX−XXX

(36) Koster, M. I.; Kim, S.; Mills, A. A.; DeMayo, F. J.; Roop, D. R. p63 is the Molecular Switch for Initiation of an Epithelial Stratification Program. *Genes Dev.* **2004**, *18* (2), 126−131.
(37) Levendoski, E. E.; Leydon, C.; Thibeault, S. L. Vocal Fold Epithelial Barrier in Health and Injury: A Research Review. *J. Speech Lang Hear Res.* **2014**, *57* (5), 1679−1691.
(38) Yánez-Soto, B.; Leonard, B. C.; Raghunathan, V. K.; Abbott, N. L.; Murphy, C. J. Effect of Stratification on Surface Properties of Corneal Epithelial Cells. *Invest. Ophthalmol. Visual Sci.* **2015**, *56* (13), 8340−8348.
(39) Houghton, O.; McCluggage, W. G. The Expression and Diagnostic Utility of p63 in the Female Genital Tract. *Adv. Anat. Pathol.* **2009**, *16* (5), 316−21.
(40) Squier, C. A.; Kremer, M. J. Biology of Oral Mucosa and Esophagus. *J. Natl. Cancer Inst. Monogr.* **2001**, *2001* (29), 7−15.
(41) Suzuki, T. Regulation of Intestinal Epithelial Permeability by Tight Junctions. *Cell. Mol. Life Sci.* **2013**, *70* (4), 631−659.
(42) Hasegawa, H.; Fujita, H.; Katoh, H.; Aoki, J.; Nakamura, K.; Ichikawa, A.; Negishi, M. Opposite Regulation of Transepithelial Electrical Resistance and Paracellular Permeability by Rho in Madin-Darby Canine Kidney Cells. *J. Biol. Chem.* **1999**, *274* (30), 20982−8.
(43) Sivasankar, M.; Erickson, E.; Rosenblatt, M.; Branski, R. C. Hypertonic Challenge to Porcine Vocal Folds: Effects on Epithelial Barrier Function. *Otolaryngol.–Head Neck Surg.* **2010**, *142* (1), 79−84.
(44) Rees, L. E.; Gunasekaran, S.; Sipaul, F.; Birchall, M. A.; Bailey, M. The Isolation and Characterisation of Primary Human Laryngeal Epithelial Cells. *Mol. Immunol.* **2006**, *43* (6), 725−730.
(45) Paszek, M. J.; Zahir, N.; Johnson, K. R.; Lakins, J. N.; Rozenberg, G. I.; Gefen, A.; Reinhart-King, C. A.; Margulies, S. S.; Dembo, M.; Boettiger, D.; Hammer, D. A.; Weaver, V. M. Tensional Homeostasis and the Malignant Phenotype. *Cancer Cell* **2005**, *8* (3), 241−254.
(46) Janmey, P. A.; Winer, J. P.; Murray, M. E.; Wen, Q. The Hard Life of Soft Cells. *Cell Motil. Cytoskeleton* **2009**, *66* (8), 597−605.
(47) Zarkoob, H.; Bodduluri, S.; Ponnaluri, S. V.; Selby, J. C.; Sander, E. A. Substrate Stiffness Affects Human Keratinocyte Colony Formation. *Cell. Mol. Bioeng.* **2015**, *8* (1), 32−50.
(48) Gouveia, R. M.; Vajda, F.; Wibowo, J. A.; Figueiredo, F.; Connon, C. J. YAP, ΔNp63, and β-Catenin Signaling Pathways Are Involved in the Modulation of Corneal Epithelial Stem Cell Phenotype Induced by Substrate Stiffness. *Cells* **2019**, *8* (4), 347.
(49) Dion, G. R.; Jeswani, S.; Roof, S.; Fritz, M.; Coelho, P. G.; Sobieraj, M.; Amin, M. R.; Branski, R. C. Functional Assessment of the ex vivo Vocal Folds through Biomechanical Testing: A Review. *Mater. Sci. Eng., C* **2016**, *64*, 444−453.
(50) Garrett, C. G.; Coleman, J. R.; Reinisch, L. Comparative Histology and Vibration of the Vocal Folds: Implications for Experimental Studies in Microlaryngeal Surgery. *Laryngoscope* **2000**, *110* (5), 814−824.
(51) Tang, S. S.; Mohad, V.; Gowda, M.; Thibeault, S. L. Insights Into the Role of Collagen in Vocal Fold Health and Disease. *J. Voice.* **2017**, *31* (5), 520−527.
(52) Teller, S. S.; Farran, A. J.; Xiao, L.; Jiao, T.; Duncan, R. L.; Clifton, R. J.; Jia, X. High-frequency Viscoelastic Shear Properties of Vocal Fold Tissues: Implications for Vocal Fold Tissue Engineering. *Tissue Eng., Part A* **2012**, *18* (19−20), 2008−19.
(53) Dicker, K. T.; Gurski, L. A.; Pradhan-Bhatt, S.; Witt, R. L.; Farach-Carson, M. C.; Jia, X. Hyaluronan: a simple polysaccharide with diverse biological functions. *Acta Biomater.* **2014**, *10* (4), 1558−70.
(54) Brown, A. C.; Rowe, J. A.; Barker, T. H. Guiding Epithelial Cell Phenotypes with Engineered Integrin-specific Recombinant Fibronectin Fragments. *Tissue Eng., Part A* **2011**, *17* (1−2), 139−50.
(55) Wang, Z.; Symons, J. M.; Goldstein, S. L.; McDonald, A.; Miner, J. H.; Kreidberg, J. A. (Alpha)3(beta)1 Integrin Regulates Epithelial Cytoskeletal Organization. *J. Cell Sci.* **1999**, *112* (Pt 17), 2925−2935.
(56) Benoit, Y. D.; Groulx, J. F.; Gagné, D.; Beaulieu, J. F. RGD-Dependent Epithelial Cell-Matrix Interactions in the Human Intestinal Crypt. *J. Signal Transduction* **2012**, *2012*, 248759.
(57) Ikemoto, S.; Mochizuki, M.; Yamada, M.; Takeda, A.; Uchinuma, E.; Yamashina, S.; Nomizu, M.; Kadoya, Y. Laminin Peptide-conjugated Chitosan Membrane: Application for Keratinocyte Delivery in Wounded Skin. *J. Biomed. Mater. Res., Part A* **2006**, *79* (3), 716−722.
(58) Nomizu, M.; Kim, W. H.; Yamamura, K.; Utani, A.; Song, S.-Y.; Otaka, A.; Roller, P. P.; Kleinman, H. K.; Yamada, Y. Identification of Cell Binding Sites in the Laminin α1 Chain Carboxyl-Terminal Globular Domain by Systematic Screening of Synthetic Peptides. *J. Biol. Chem.* **1995**, *270* (35), 20583−20590.
(59) Yamada, Y.; Hozumi, K.; Katagiri, F.; Kikkawa, Y.; Nomizu, M. Laminin-111-Derived Peptide-Hyaluronate Hydrogels as a Synthetic Basement Membrane. *Biomaterials* **2013**, *34* (28), 6539−6547.
(60) Tata, P. R.; Mou, H.; Pardo-Saganta, A.; Zhao, R.; Prabhu, M.; Law, B. M.; Vinarsky, V.; Cho, J. L.; Breton, S.; Sahay, A.; Medoff, B. D.; Rajagopal, J. Dedifferentiation of Committed Epithelial Cells into Stem Cells in vivo. *Nature* **2013**, *503* (7475), 218−223.
(61) Duffield, J. S.; Park, K. M.; Hsiao, L. L.; Kelley, V. R.; Scadden, D. T.; Ichimura, T.; Bonventre, J. V. Restoration of Tubular Epithelial Cells during Repair of the Postischemic Kidney Occurs Independently of Bone Marrow-derived Stem Cells. *J. Clin. Invest.* **2005**, *115* (7), 1743−55.
(62) White, C. E.; Kwok, B.; Olabisi, R. M. Activin A improves Retinal Pigment Epithelial Cell Survival on Stiff but not Soft Substrates. *J. Biomed. Mater. Res., Part A* **2018**, *106* (11), 2871−2880.
(63) Tash, J. A.; David, S. G.; Vaughan, E. E.; Herzlinger, D. A. Fibroblast Growth Factor-7 Regulates Stratification of the Bladder Urothelium. *J. Urol.* **2001**, *166* (6), 2536−2541.
(64) Nakajima, T.; Hayashi, S.; Iguchi, T.; Sato, T. The Role of Fibroblast Growth Factors on the Differentiation of Vaginal Epithelium of Neonatal Mice. *Differentiation* **2011**, *82* (1), 28−37.
(65) Nguyen, N.; Fernando, S. D.; Biette, K. A.; Hammer, J. A.; Capocelli, K. E.; Kitzenberg, D. A.; Glover, L. E.; Colgan, S. P.; Furuta, G. T.; Masterson, J. C. TGF-β1 Alters Esophageal Epithelial Barrier Function by Attenuation of Claudin-7 in Eosinophilic Esophagitis. *Mucosal Immunol.* **2018**, *11* (2), 415−426.
(66) Rodriguez, P.; Da Silva, S.; Oxburgh, L.; Wang, F.; Hogan, B. L.; Que, J. BMP Signaling in the Development of the Mouse Esophagus and Forestomach. *Development* **2010**, *137* (24), 4171−4176.

https://dx.doi.org/10.1021/acsbiomaterials.0c01741
ACS Biomater. Sci. Eng. XXXX, XXX, XXX−XXX